pubs.acs.org/JPCC

Article

Structure and Dynamics of Perylene Bisimide Pigments for "Cool" Organic Coatings by Solid-State NMR: A Combined Experimental and DFT Study

Francesca Martini,* Marco Geppi,* Giovanni Barcaro, Susanna Monti, Luca Contiero, Giacomo Ruggeri, Marco Lessi, Andrea Pucci, Fabio Bellina, and Silvia Borsacchi

Read Online

ACCESS | Metrics & More | Article Recommendations | Supporting Information

ABSTRACT: In this work, a combination of high-resolution solid-state nuclear magnetic resonance (SSNMR) experiments and density functional theory calculations has been exploited for obtaining a detailed characterization of the structural and dynamic properties of the perylene bisimide derivative (PBI) Paliogen Black L0086 (P-black). This "cool" organic pigment is characterized by unusual transparent, reflective, and cooling features in the near-infrared (NIR) spectrum. A full assignment of the ^{13}C SSNMR spectrum was achieved, highlighting correlations between ^{13}C isotropic chemical shifts and specific supramolecular features. The π-flip motion of the phenyl rings of the methoxybenzyl side groups bonded to the imide nitrogen atoms was characterized in the 310−386 K temperature range, determining activation energy and correlation times. This motion showed a strong dependence on the supramolecular order of P-black and the length of the alkyl linker between the side group and the perylene bisimide core. The results obtained in this work open the way to investigations on similar PBI pigments, aiming at achieving a collection of molecular, supramolecular, and NIR data that could allow the identification of the main factors determining the NIR performance.
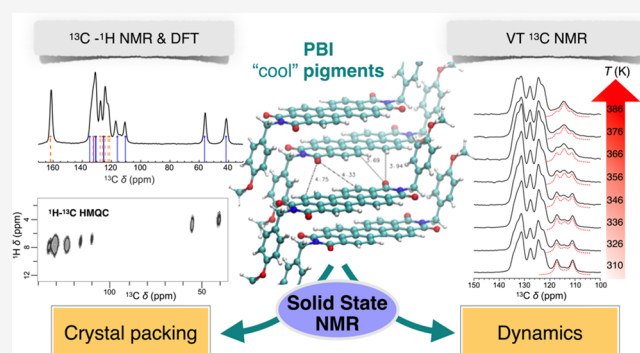
1. INTRODUCTION

In the past decade, perylene bisimide derivatives (PBIs) have aroused a considerable interest for the design of functional materials with many different applications, from the production of organic electronic devices, such as organic solar cells,[1] organic light-emitting diodes,[2] and field-effect transistors,[3,4] to their use as dyes in luminescent solar concentrators[5−9] and smart polymeric materials.[10,11] Besides, PBIs have extensively been used for the development of high-performance industrial pigments, thanks to their excellent tinctorial strength, insolubility, weather resistance, and chemical stability, as well as to the possibility of obtaining a wide variety of colors and optical properties by varying the substituents at the peripheral positions of the PBI core.[11−13] Recently, considerable interest has been addressed to the reflectivity and transparency properties of PBIs in the near-infrared (NIR) region of the electromagnetic spectrum, which make them promising candidates as "cool" organic pigments.[14−16] Nowadays, painting building roofs and façades with coatings based on "cool" pigments, which mimic the NIR reflective and transparent properties of certain green plants,[17] is one of the most accessible strategies to reduce the warming induced by the sunlight exposure,[18−21] which is mainly due to the absorption of the NIR components of the solar emission

spectrum. It has been demonstrated that this approach is effective in reducing the urban heat island effect[22−24] and the related high-energy demands in densely populated urban regions, as required by the EU regulation in the 2010/31/EU Directive. In this context, PBIs represent a more versatile and lower-cost alternative to inorganic pigments,[19,25] such as chromium, titanium, and rare-earth oxides, which currently dominate the market of "cool" pigments. In a recent study,[26] Paliogen Black L0086 (P-black) (Figure 1), a black commercial PBI, has been successfully used in combination with thermoplastic hollow microspheres to produce NIR-reflective acrylic coatings, leading to striking NIR and solar reflectances of more than 45 and 22%, respectively. However, in most cases, the optical behavior in the NIR region of PBIs is still inferior to that of inorganic compounds, and further
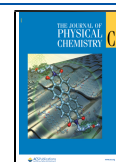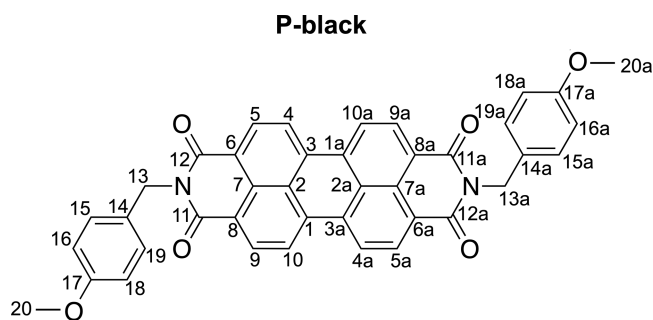
P-black

Figure 1. Molecular structure of P-black with the carbon numbering used throughout the paper.

research efforts are necessary before scaling up their application.

The design of materials with improved and optimized performance cannot be separated from a deep comprehension of the structure−property relationships. The interaction with the NIR radiation has been studied for a large number of N,N′-disubstituted PBI pigments, which usually displayed a combination of NIR transparent and reflective properties that were strongly connected to the nature of the substituents.[14,16,27,28] Indeed, depending on the type and position of the functionalizations of the perylene bisimide core, PBIs form a wide variety of crystalline structures, where the different molecules are assembled through π−π stacking interactions,[29,30] in ordered and sometimes disordered orientations.[16,31] The correlations between the optical properties in the NIR region and the morphological features of PBIs, such as pigment particle size, crystallinity, supramolecular packing, and dipole moment, have been investigated,[14,16,27,28,31,32] but a clear and full understanding is still lacking. In an earlier investigation,[31] it has been demonstrated that the increase of the structural order in the supramolecular packing of P-black leads to an essential improvement of the NIR reflectivity and cooling properties of acrylic coatings. Similar to the well-known crystallochromy effect,[29,33] the absorption, transparency, and reflectance of PBIs in the NIR region seem to be deeply rooted in the characteristics of the crystal packing in the solid state, which determine the electronic structure and, therefore, the refractive index of these materials. However, for many of these compounds, the crystallographic structure is not available because of the difficulties encountered in obtaining single crystals of good quality.

Solid-state NMR spectroscopy (SSNMR) can disclose molecular properties and supramolecular packing of these materials by exploiting the sensitivity of many nuclear properties to conformational features, intermolecular interactions, spatial proximities, and dynamics in solid materials.[34] Moreover, as witnessed by the established field of NMR "crystallography",[35,36] the interpretation of the structural information can be refined by resorting to density functional theory (DFT) calculations. Remarkably, SSNMR has practically no limitations regarding the kind of sample, which can be amorphous, crystalline or semicrystalline, or single- or multicomponent. This can be particularly useful in the field of "cool" pigments, allowing, for instance, the study of pigments in a final coating. In recent years, the combination of advanced ^{1}H high-resolution SSNMR experiments and DFT calculations has been successfully used, in support of other characterizations, to investigate the self-assembling properties of PBI derivatives

with application in optoelectronics.[37−41] However, despite this great potential, so far the use of SSNMR to the study of "cool" PBI pigments has been quite limited.

Recently, the preliminary ^{13}C SSNMR spectra of P-black revealed sensitivity to the supramolecular packing of this pigment.[31] Although the intricate overlapping of signals, especially in the aromatic region, prevented a full assignment of the ^{13}C spectrum, a specific "dynamic disorder", involving the side groups bonded to the imide nitrogen atoms, was revealed, which showed an interesting correspondence with a particular structural disorder on the nanometric scale. In turn, such a disorder resulted in inferior NIR reflective properties.

Motivated by the general interest in this class of pigments and the potential of SSNMR, we carried out a combined ^{13}C and ^{1}H SSNMR and DFT study on P-black, with the purpose of understanding and characterizing its structural and dynamic properties in the solid state. The final aim of this work is dual. On the one hand, a full assignment of the ^{13}C SSNMR signals of P-black, for which the crystal structure is known,[29,30] will allow the detection of specific correlations between SSNMR and structural features, which could be useful for PBI pigments whose crystal structure is not available. On the other hand, an in-depth characterization of the active molecular dynamic processes, for which SSNMR is the method of choice, is fundamental and could open the way to the characterization of similar compounds. Indeed, in the final part of the paper, through a preliminary investigation on PBI pigments similar to P-black, we will show how the achieved knowledge on P-black can be transferred to slightly different compounds, allowing us to gain information on their structural and dynamic features directly from the ^{13}C SSNMR spectra. The definition of an effective SSNMR approach for the characterization of this class of pigments is important in the perspective of collecting molecular data that, compared with supramolecular features and NIR performances, can help to understand the relations between "micro-" and "macro-" scale properties.

2. MATERIALS AND METHODS

2.1. Materials. The commercially available Paliogen Black L0086 (P-black) and Paliogen Black S0084 (P-black S0084) pigments were provided by BASF and used without further purification. The synthetic P-black (P-black-S), Pigment Red 190 (PR-190), and Paliogen Black L0096 (P-black L0096) were prepared according to a recently published procedure[31] in 96, 53, and 98% yields, respectively.

2.2. Experimental Methods. ^{13}C SSNMR experiments were carried out on a Varian InfinityPlus 400 spectrometer, working at ^{1}H and ^{13}C Larmor frequencies of 400.35 and 100.67 MHz, respectively. All of the measurements were performed using a 3.2 mm cross-polarization/magic angle spinning (CP/MAS) probe head, accommodating rotors with an outer diameter of 3.2 mm, by spinning the samples at the MAS frequency of 15 kHz. The 90° pulse durations were 1.8 and 2.7 μs for ^{1}H and ^{13}C nuclei, respectively. A SPINAL-64[42] pulse sequence for high-power decoupling of ^{13}C nuclei from ^{1}H ones was applied during signal acquisition, at the decoupling field of 87 kHz. ^{13}C CP/MAS spectra were acquired with contact times (ct) of 0.05 and 2 ms using a linear ramp for the ^{13}C cross-polarization field. Scans (6000−12,000) were accumulated. ^{13}C non quaternary suppression (NQS)[43] spectra were recorded by introducing a delay of 100 μs between the CP pulses and acquisition by collecting 11,000 transients. ^{1}H−^{13}C MAS-J-HMQC (heteronuclear multiple-

$d_1 = 4.75$ Å $(O_1 - 5)$
$d_2 = 4.33$ Å $(O_1 - 9)$
$d_3 = 3.69$ Å $(O_2 - 10)$
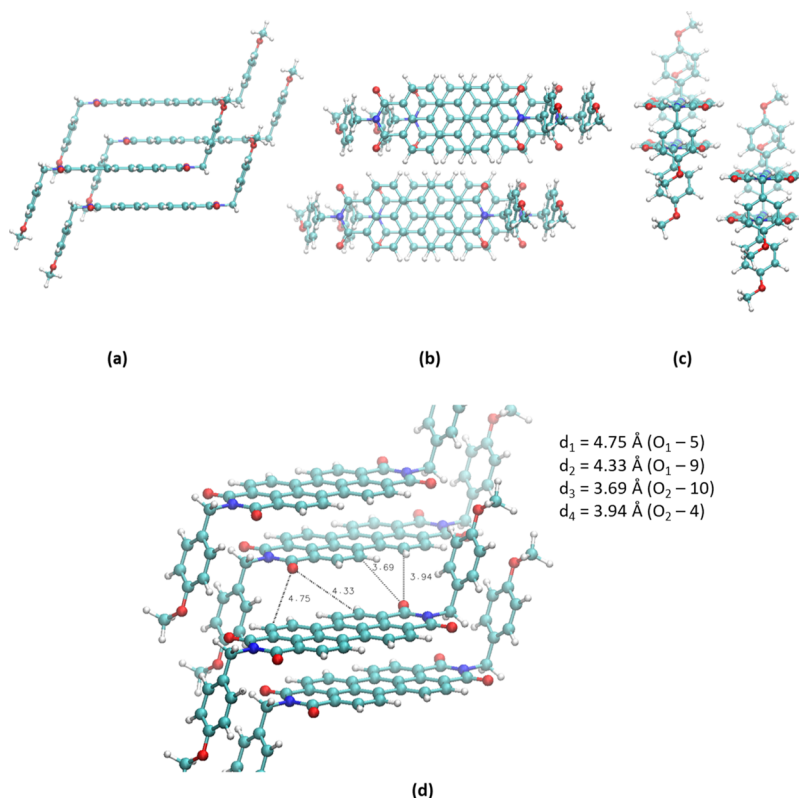$d_4 = 3.94$ Å $(O_2 - 4)$

Figure 2. P-black molecule replicated in a (2×2) cell; (a−c) three different views highlighting the mutual orientations inside the crystalline packing; (d) side view with some characteristic C−O distances (between atoms belonging to neighboring molecules).

quantum coherence) experiments were carried out using the pulse scheme described in ref 44 at the MAS frequency of 19.53 kHz and using a ct of 1 ms for CP. Increments (128) were collected in the second dimension, with a dwell time of 23.04 μs and adding two FSLG cycles per increment. The ^{1}H rf field during FSLG was about 120 kHz. For each increment, 272 transients were accumulated. In all experiments, a recycle delay of 5 s between consecutive transients was used. Air was used as heating and spinning gas. To take into account the frictional heating of the sample under MAS, the temperature inside the rotor was calibrated using the ^{207}Pb isotropic chemical shift (CS) in Pb(NO$_3$)$_2$ following the procedure described in ref 45. When not differently specified, the experiments were carried out at a nominal temperature of 295 K, which, at the MAS frequency of 15 kHz, corresponded to a real temperature of the sample of 310 K. The ^{13}C CS scale was referenced to the ^{13}C signals of tetramethyl silane and hexamethylbenzene, which are used as primary and secondary references, respectively.

2.3. Computational Methods. DFT calculations have been performed by using the Quantum Espresso (QE) suite of programs,[46] with plane-wave basis sets and periodic boundary conditions in a cell, determined by the experimental crystallographic data,[30] containing a single P-black molecule of 74 atoms. By fixing the lattice constants of the unit cell to the experimental ones, we have considered the crystallographic positions of the molecules and locally optimized the coordinates of all of the atoms at the DFT level by using plane-augmented-wave (PAW) pseudopotentials and the PBE-D2 XC-functional.[47,48] Cutoffs on the wave function and electronic density were set to 80/800 Ry (1 Ry = 1312.75 kJ/mol), and the first Brillouin cell in the reciprocal space has

been sampled according to a $(4 \times 2 \times 1)$ mesh of k points. Calculations were performed spin-restricted by applying Gaussian smearing of the one-particle energy levels of 0.002 Ry. NMR CSs were simulated by using the gauge including PAW (GIPAW) approach[49] implemented in QE.

In Figure 2a, the (2×2) replica of the unit cell shows the mutual orientation of the P-black molecules inside the crystalline packing. In Figure 2b (direction perpendicular to the perylene plane), it is apparent that the molecules adopt the staggering stacking characteristic of graphite. In Figure 2d, some characteristic distances between C and O atoms belonging to neighboring molecules have been highlighted to show the loss of symmetry between pairs of atoms which, in the isolated molecule, would be equivalent. This is the case, for example, of the 4−10 (distances of 3.69 and 3.94 Å, respectively) and 5−9 (distances of 4.75 and 4.33 Å, respectively) pairs.

3. RESULTS AND DISCUSSION

3.1. Assignment of the ^{13}C NMR Spectrum of P-Black. As noted earlier,[26,31] the ^{13}C CP/MAS spectrum of P-black is very complex, especially in the aromatic region, where many different carbon signals overlap at values of CS that are likely influenced by the local environment determined by the supramolecular packing of the molecules. In the following, we report the full assignment of the ^{13}C CP/MAS spectrum of P-black, carried out combining ^{13}C-selective experiments and DFT calculations.

^{13}C-selective experiments can be extremely beneficial for the analysis of a complex spectrum, like that of P-black. Here, we performed experiments based on the alternative detection of either quaternary or nonquaternary carbons. In particular, a

^{13}C CP/MAS spectrum with a very short ct of 0.05 ms was recorded to selectively observe the signals of nonquaternary carbons, whereas the signals of quaternary carbons were relatively enhanced by performing ^{13}C NQS experiments. The selective spectra obtained for P-black are shown in Figure 3a, compared with the ^{13}C CP/MAS spectrum recorded with ct = 2 ms, where all of the carbon signals are present.
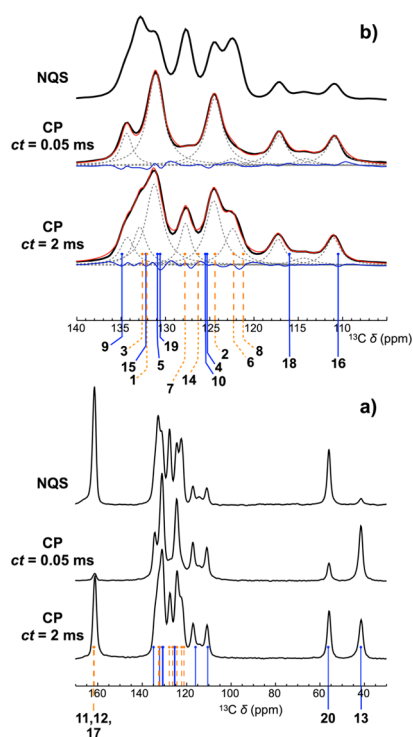

Figure 3. (a) ^{13}C CP/MAS (ct = 0.05 and 2 ms) and NQS spectra of P-black. (b) Expansions of the 105−140 ppm region of the spectra reported in (a). For the ^{13}C CP/MAS spectra, the results of the spectral fitting are also reported: experimental spectra (black lines), fitted curves (red lines), single peaks (dotted dashed lines), residuals (blue lines). The vertical lines point out the values of CS (δ_{iso}^{calc}) obtained from DFT calculations for the different quaternary (orange) and nonquaternary (blue) X/Xa carbons (simply indicated as X).

Using the carbons numbering reported in Figure 1, ^{13}C signals at 41.5 and 56.0 ppm are easily assigned to C̲H$_2$ (13/13a) and OC̲H$_3$ (20/20a) carbons, respectively, whereas the peak at 161.4 ppm is ascribable to C̲O (17/17a) and NC̲=O (11/11a and 12/12a) carbons. The fact that X and Xa carbons resonate at the same value of CS is in agreement with the symmetry of the crystal structure of P-black determined by single-crystal X-ray diffraction (XRD),[30] which has an inversion center in the center of mass of the molecule, with a single molecule in the unit cell. Given this symmetry, from now on, carbons X/Xa will be simply indicated as X. For the assignment of the intricate aromatic region (between 105 and 140 ppm), it was useful to perform a spectral fit with the minimum number of peaks, ensuring a sound reproduction of the experimental profile. The results are reported in Figure 3b and in Tables S1 and S2. For the spectrum at ct = 2 ms, a satisfactory fit was obtained using a sum of 10 peaks. It must be noticed that the peaks are quite broad with respect to what expected for a crystalline phase, indicating the presence of a distribution of isotropic CSs because of a certain degree of local structural disorder. The peaks at 110.9, 114.2, and 117.2

ppm arise from carbons 16 and 18 in different structural environments. In particular, the signals of almost equal intensity at 110.9 and 117.2 ppm are ascribed to molecules for which a fixed conformation of the methoxyphenyl group determines the inequivalence of the signals of carbons 16 and 18. On the contrary, the peak at 114.2 ppm is due to a motion rapidly exchanging the positions 16 and 18, which was already identified with the fast π-flip of the phenyl ring.[31] By comparing the different selective spectra, it is evident that the remaining CH carbons, belonging to the PBI core (4, 5, 9, and 10) and to the phenyl ring (15 and 19), give rise to signals at 124.4, 131.1, and 134.4 ppm. Indeed, these signals are strongly enhanced in the CP spectrum at ct = 0.05 ms and depressed in the NQS one (Figure 3b, Tables S1 and S2). Conversely, signals that are undoubtedly ascribed to quaternary carbons are those at 122.4, 127.7, and 132.9 ppm. This assignment was further corroborated by a ^{1}H−^{13}C HMQC spectrum (vide infra).

In order to go into more detail in the analysis of the ^{13}C SSNMR spectra, we performed DFT calculations. The assignment of all ^{13}C signals of P-black, as obtained by combining SSNMR experiments and the DFT calculations, is reported in Table 1 and is visually displayed on the ^{13}C CP/

Table 1. Assignment of the ^{13}C Signals of P-Black As Obtained from the Joint Analysis of ^{13}C CP/MAS-Selective Spectra and DFT Calculations[a]

carbon	δ_{iso}^{calc}	δ_{iso}^{exp}
13	41.6	41.5
20	56.3	56.0
16	110.5	110.9
18	116.0	117.2
8	121.3	122.4
6	122.3	
2	124.4	124.6
4	125.3	
10	125.5	
14	126.3	127.7
7	127.8	
19	130.6	131.3
5	130.9	
15	132.2	
1	132.1	132.9
3	132.6	
9	134.9	134.3
12	161.6	161.4
11	161.8	
17	161.9	

[a]For each P-black carbon, the calculated (δ_{iso}^{calc}) and experimental (δ_{iso}^{exp}) values of the isotropic CSs are reported. The error on δ_{iso}^{exp} is ±0.2 ppm. RMSD is 0.68 ppm.

MAS spectrum reported in Figure 3b. The excellent agreement between experimental and calculated CSs and the use of SSNMR-selective experiments make this assignment sound and complete. In Table S3 of the Supporting Information, we compare the calculated ^{13}C isotropic CSs (δ_{iso}^{calc}) for P-black as an isolated molecule and in the crystal. As expected, δ_{iso}^{calc} values largely differ in these two situations: in the crystal, all of the quaternary carbons of the PBI core (1, 2, 3, 6, 7, 8) are shielded by 2−3 ppm with respect to the isolated molecule, while most of the nonquaternary carbons of the core (4, 9, 10)
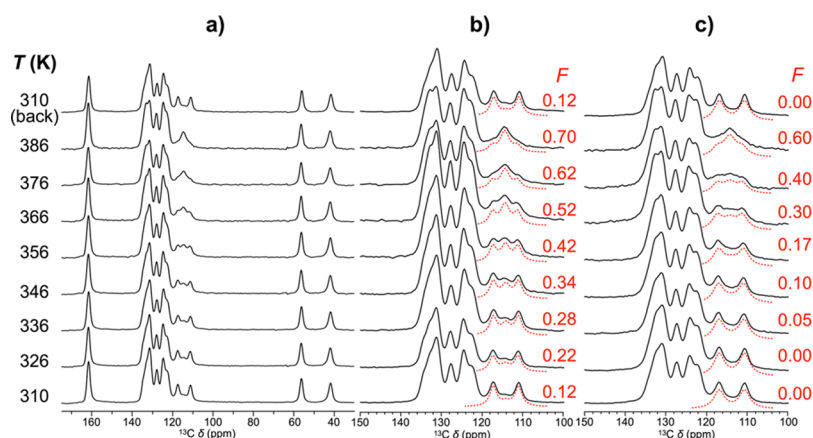
Figure 4. (a) ^{13}C CP/MAS spectra (ct = 2 ms) of P-black, recorded at different temperatures from 310 to 386 K. The experimental temperatures (T, K) are indicated on the left. The first spectrum from the top has been acquired at the temperature of 310 K after cooling back the sample from 386 K. (b,c) Expansions of the 100−150 ppm spectral region of the ^{13}C CP/MAS spectra of P-black (b) and P-black-S (c). The dashed red lines represent the simulated line shapes for the signals of the exchanging carbons 16 and 18 obtained as described in the main text using a linewidth of 210 Hz for the individual lines. The values of the fraction of the fast component (F) obtained from the simulations are reported on the right of the spectra.

are deshielded by about 4 ppm. These variations are due to molecular packing and in particular can be ascribed to the transversal and longitudinal shifts between adjacent molecules in the same columnar stacks. Specifically, all of the quaternary carbons fall within the shielding cone of the aromatic core of the closest molecules in the columnar stack, whereas the nonquaternary carbons are all in a deshielding region (Figure 2).

The assignment of the ^{13}C spectrum of P-black deserves some comments. Notably, calculations well reproduce the different CSs of carbons 16 and 18, which are related to the orientation assumed by the OCH$_3$ group, with the carbon atom lying nearly in the plane of the phenyl ring:[30] in particular, the interaction with the hydrogen atoms of the methyl group determines a magnetic shielding of carbon 16 (Figure 2).

A minor splitting was calculated for the signals of carbons 15 and 19 in meta position with respect to the OCH$_3$ group, which are less affected by its orientation. In the experimental spectrum, however, it is probable that both these carbons contribute to the peak at 131 ppm. Similarly, carbons 1 (δ_{iso}^{calc} = 132.1 ppm) and 3 (δ_{iso}^{calc} = 132.6 ppm) can both be associated with the signal at 132.9 ppm, which has been ascribed to quaternary carbons (Figure 3b). Remarkably, DFT calculations predict different values of isotropic CS for the CH carbons of the PBI cores 4 (δ_{iso}^{calc} = 125.3 ppm), 10 (δ_{iso}^{calc} = 125.5 ppm), 5 (δ_{iso}^{calc} = 130.9 ppm), and 9 (δ_{iso}^{calc} = 134.9 ppm), in very good agreement with the experimental ^{13}C spectra. In fact, these carbons can account for the three peaks at 124.4 (4 and 10), 131.1 (5), and 134.4 (9) ppm in the ^{13}C CP/MAS spectrum at ct = 0.05 μs. The relative areas of these peaks (Table S2) further support this assignment, considering the additional contribution of carbons 15 and 19 to the signal at 131.1 ppm. Indeed, although it is known that CP spectra are not quantitative,[50] it is also reasonable that CH carbons in similar chemical and structural environments are characterized by similar cross-polarization efficiencies. The significant difference between the isotropic CS of carbons 5 and 9 is in agreement with the fact that the crystallographic structure is not symmetric with respect to the longitudinal bisecting vector through the PBI core,[30] as shown in Figure 2. This result

clearly shows that the ^{13}C isotropic CSs of the carbons of the PBI core can be very sensitive to the transverse shift between two adjacent PBI molecules within the same columnar stack, a structural parameter that is known to strongly affect the electronic and optical properties of these pigments in the solid state.[29]

The SSNMR spectral assignment of P-black was also completed with the analysis of ^1H data. To this aim, a $^1H-^{13}C$ HMQC bidimensional spectrum, where cross-peaks between directly bonded ^1H and ^{13}C nuclei can be observed, was recorded (Figure S1). The signals of hydrogen nuclei of methoxy group, alkyl linker, phenyl ring, and perylenic core could be distinguished, and the experimental values of the CSs resulted in very good agreement with those obtained from DFT calculations (Table S4). However, the slightly different isotropic CS values found by DFT for the different ^1H nuclei of the perylene core could not be experimentally discerned because of the insufficient spectral resolution in the ^1H dimension, possibly resulting from the structural heterogeneity of the sample and residual $^1H-^1H$ dipolar interactions. A more detailed description of the results is reported in the Supporting Information.

3.2. Dynamics of P-Black at Variable Temperatures. As already stated, although the PBI core of P-black is very rigid, the external methoxyphenyl groups can exhibit a π-flip of the phenyl ring about its para axis.[31] To better characterize such a dynamic process, we recorded the ^{13}C CP/MAS spectra of P-black at different temperatures, from 310 to 386 K (Figure 4). By looking at Figure 4a, it is indeed evident that most of the spectrum remains unchanged with increasing temperature with the remarkable exception of the region between 108 and 120 ppm, where the signals of carbons 16 and 18 resonate. On heating, we can observe a gradual transformation from a shape dominated by a doublet (111 and 117 ppm, because of carbons 16 and 18, respectively, in a frozen conformation) to the one where a singlet at the average CS of 114 ppm prevails. The latter can be straightforwardly assigned to carbons 16 and 18 in "fast" exchange, that is, in molecules where the π-flip motion of the phenyl ring has a characteristic frequency much larger than the splitting of the doublet (Δν ≈ 600 Hz). Accordingly, minor changes also occur on heating in the spectral region

around 131 ppm, where the signals of carbons 15 and 19 resonate, even exchanging their positions during the π-flip of the phenyl ring.

Nevertheless, a visual inspection of the trend of the spectral shape versus temperature clearly indicates that this motion cannot be described by a simple coalescence process, expected in the presence of a single correlation time (τ_c), because situations of fast and slow exchange coexist at all investigated temperatures. To obtain a detailed and quantitative description of this motional process, we carried out simulations of the significant spectral region between 104 and 124 ppm over the whole investigated range of temperatures by making use of a motional model taking into account a distribution of correlation times. In particular, we used the William−Watts model,[51] where the autocorrelation function of the motion $g(t)$ is nonexponential and, in particular, contains a distribution of τ_c (eq 1).

$$g(t) \propto e^{-(t/\tau_p)^\alpha} \tag{1}$$

The breadth of the distribution is described by the parameter α ($0 \leq \alpha \leq 1$, the two extremes corresponding to the limiting situations of flat distribution and single correlation time, respectively), whereas its position on the time axis is expressed by the parameter τ_p. Such a model already revealed effective to describe an inhomogeneous distribution of dynamic environments related to the presence of a certain degree of structural disorder in solid materials.[52−54]

The Williams−Watts model was used in combination with the McConnell equations,[55] suitable to reproduce exchange phenomena between two equally populated sites with different resonance frequencies, such as those associated with the π-flip motion of the phenyl ring. In particular, because it was clear that a broad distribution of correlation times was necessary to reproduce the experimental spectra, we used the approximation suggested by Garroway et al. in the case of $\alpha \leq 0.3$.[53] This consists of neglecting the contribution from molecules in the intermediate motional regime[56] and therefore assumes that the experimental lineshapes can be reproduced as the weighted sum of the lineshapes arising from one *fast* and one *slow* component, respectively, characterized by a τ_c much shorter and much longer than the coalescence correlation time $\tau_m = \sqrt{2}/(\pi\Delta\nu)$, of the order of 1 ms.

In Figure 4b, an expansion of the 104−124 ppm spectral region of the variable temperature ^{13}C CP/MAS spectra is shown together with the above-described simulations, which provide a very satisfactory reproduction of the experimental behavior. The obtained results show that the fraction of the fast component (F) in the simulated line shape (characterized by values of τ_c much shorter than τ_m) progressively increases by increasing temperature. Within the frame of the broad distribution of τ_c used ($\alpha \leq 0.3$) and considering an Arrhenius dependence of τ_p on temperature ($\tau_p = \tau_\infty\, e^{E_a/RT}$), the following relation between F and the parameters of the motion holds true[53]

$$\ln[\ln(1 - F)^{-1}] = \alpha \ln \frac{\tau_m}{\tau_p} = \alpha\left[\ln \frac{\tau_m}{\tau_\infty} - \frac{E_a}{RT}\right] \tag{2}$$

where τ_∞ and E_a are, respectively, the pre-exponential factor (correlation time at infinite temperature) and the activation energy of the motion.

By plotting the values of $\ln[\ln(1 - F)^{-1}]$ obtained from simulations vs $1000/T$ (Figure 5), a linear trend was found, in
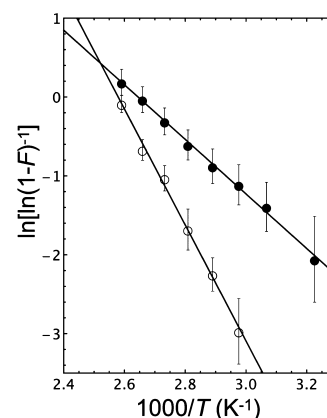

Figure 5. Plot of $\ln[\ln(1 - F)^{-1}]$ obtained from the simulation of the 104−124 ppm ^{13}C spectral regions of P-black (filled circles) and P-black-S (empty circles) as a function of temperature. The fitting curves obtained by a linear least-square fitting to eq 2 are also reported (black lines). 9.1 and 19.6 were found as best-fitting y-intercepts for P-black and P-black-S, respectively, while the corresponding best-fitting slopes are −3.46 and −7.35 K^{-1}.

good agreement with the predicted behavior. When $T \simeq 378$ K, the value of $\ln[\ln(1 - F)^{-1}]$ approaches zero: at this point, independent of α, $\tau_p \simeq \tau_m \simeq 1$ ms. From a linear fitting of the experimental data, we found $\alpha E_a = 29$ kJ/mol (Figure 5). Because $\alpha \leq 0.3$, this indicates that $E_a \geq 97$ kJ/mol for the exchange motion. This value is in the range (20−150 kJ/mol) of activation energies commonly found in the literature for π-flip movements of aromatic rings,[53,57−61] being comparable with those previously measured for tyrosine residues characterized by strong aromatic−pair interactions in proteins.[59,60] This finding appears in agreement with the tight packing of P-black molecules through $\pi−\pi$ stacking interactions, which could sharply increase the activation energy of the flip motion of the phenyl side-groups.

Finally, it is interesting to compare these results with those obtained for P-black-S, the synthetic form of the commercially available P-black (Figures 4c and S2). In a previous work,[31] P-black-S was found to have a higher structural order than P-black and to be formed by crystallites of greater mean size. A spectral simulation at variable temperature similar to that above described for P-black was also performed for P-black-S (Figure 4c). Also in this case, a linear trend was found for $\ln[\ln(1 - F)^{-1}]$ versus $1000/T$ (Figure 5), in agreement with the presence of a broad ($\alpha \leq 0.3$) and inhomogeneous distribution of τ_c and an Arrhenius dependence of τ_p on temperature. However, an overall slowing down of the exchange motion in the investigated temperature range is evident, as indicated by the much smaller values of F (Figure 4c) and by the fact that the value of $\ln[\ln(1 - F)^{-1}]$ approaches zero ($\tau_p \simeq 1$ ms) about 10 K above with respect to P-black (Figure 5). Moreover, a much higher value of αE_a was found (61 kJ/mol, corresponding to $E_a \geq 203$ kJ/mol). Because E_a is not expected to vary significantly, this result can be explained with a higher value of α (within the limit $\alpha \leq 0.3$) relative to P-black, which implies a narrower distribution of τ_c in agreement with the overall higher structural order of P-black-S.

Finally, it should be noted that for both P-black and P-black-S, the spectra recorded after cooling back the samples to 310 K are identical to those obtained before heating (Figures 4 and
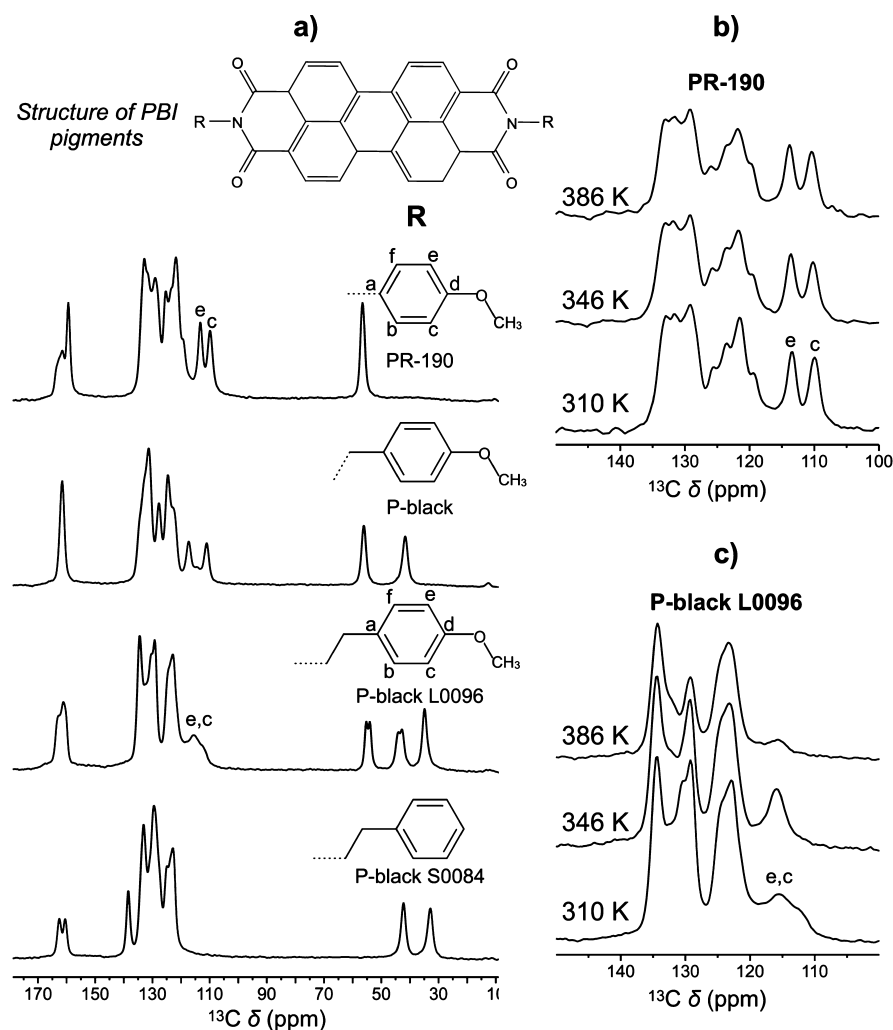
Figure 6. (a) ^{13}C CP/MAS spectra (ct = 2 ms) of the indicated PBI pigments. (b,c) Aromatic region of the ^{13}C CP/MAS spectra of PR-190 and P-black L0096, respectively, recorded at the indicated temperatures. The spectra in (b,c) provide indications on how the π-flip motion of the phenyl ring is influenced by the length of the alkyl linker: compared to P-black, the exchange between carbons e and c of the phenyl ring (signals between 105 and 120 ppm) is frozen in PR-190, even at the highest temperature of 386 K, whereas it is faster for P-black L0096, for which a large fraction of molecules is in the fast exchanging regime already at 310 K.

S2), indicating that the effects of the thermal treatment are entirely reversible.

3.3. ^{13}C Spectra of Other PBI Pigments. In the previous paragraphs, we demonstrated how the combination of ^{13}C SSNMR experiments and DFT calculations could be used to accurately relate the observed ^{13}C CSs to specific features of the crystal packing of P-black, such as the shifts between two neighboring PBI molecules in the same columnar stack and the conformational and dynamic properties of the imide substituents. With the aim of extending this approach to the characterization of other PBI pigments of unknown or uncertain crystal structures, we compared the ^{13}C CP/MAS spectrum of P-black with those of a series of PBI pigments bearing slightly different substituents at the imide positions (Figure 6a). In all cases, the substituents contain phenyl or 4-methoxyphenyl groups attached to the imide group through alkyl linkers of different lengths. In Figure 6a, we reported the ^{13}C CP-MAS spectra of P-black, P-black S0084 (whose crystal structure, determined by single-crystal XRD, is already known from the literature[29,30]), PR-190, and P-black L0096 (see Section 2.1), for which the crystal structure is unknown. It is immediately apparent that the position and the number of ^{13}C

signals strongly vary among the different compounds, especially in the aromatic region, reflecting changes not only in the chemical structure of the substituent but also in the crystal packing. For example, in the case of P-black S0084, a splitting of the C=O signal in two peaks at 160.5 and 162.5 ppm is observable. This could be due to the presence of either two inequivalent imide sites in the unit cell or, given the larger transversal shift with respect to P-black,[29] two C=O groups belonging to the same imide moiety feeling slightly different interactions with the surrounding molecules. At the moment, both the hypotheses are consistent with the available crystallographic structure.[30] The presence of structurally inequivalent molecular sites in the crystal can also be observed for P-black L0096, for which small splittings of the signals of the −OCH₃ group (at about 55 ppm) and of the −CH₂ group bonded to the imide nitrogen (at about 44 ppm) are detected. Future investigation, including DFT calculations, could better clarify these aspects.

The ^{13}C spectra of PR-190 and P-black L0096 give the opportunity to inspect if and how the dynamics of the methoxyphenyl groups is influenced by the length of the alkyl linker with the imide groups. In analogy with the signal

assignment previously performed for P-black, we can assign the signals between 105 and 120 ppm to carbons c and e (see Figure 6a). Their evolution with temperature (Figure 6b,c) clearly shows that the rate of the π-flip of the phenyl ring increases with the increase of the length of the alkyl spacer. In particular, on the NMR time scale, this motion remains frozen even at high temperatures for PR-190, for which two separate signals for carbons c and e are observed even at 386 K. On the contrary, this motion appears much faster in P-black L0096, where a large fraction of molecules is in the fast exchanging regime already at 310 K. Here, the line shape at 310 K and its change with temperature suggest the presence of a broad and inhomogeneous distribution of correlation times, similar to that previously observed for P-black and P-black-S. Notably, in the CP spectrum at 386 K, the signals of fast-exchanging c and e (116 ppm) and b and f (≈131 ppm) carbon pairs show a substantial reduction in intensity. This agrees with the high frequency of the π-flip motion, which could either weaken the $^1H-^{13}C$ dipolar interactions (thus reducing CP efficiency) or interfere with the MAS or decoupling frequencies. It is worth to notice that the strong dependence of the rate of the observed exchange phenomenon on the length of the alkyl spacer is a further confirmation that the motion under investigation is indeed the π-flip of the phenyl ring rather than the reorientation of the methoxy group because the latter would presumably be substantially unaffected by the length of the spacer.

4. CONCLUSIONS

The combination of high-resolution 1D, 2D, and selective ^{13}C and ^1H SSNMR experiments with DFT calculations of the isotropic CSs, which showed an excellent agreement with the experimental data, allowed us to assign the quite intricate SSNMR spectra of P-black. Clear correlations between the isotropic CSs, especially of the carbon nuclei of the perylenic core, and specific features of the molecular arrangement in the crystal, such as relative longitudinal and transversal shifts between P-black molecules in the columnar stacks, were recognized. Moreover, the side methoxybenzyl groups bonded at the imide nitrogen atoms showed a peculiar reorientational dynamics, which was characterized in detail over about 80 K above room temperature. The π-flip of the phenyl ring, recognized as the active motion, appeared strongly heterogeneous throughout the sample, showing a broad distribution of correlation times. The spectral simulation of the temperature evolution of the most affected signals, carried out by exploiting suitable models, allowed a quantitative estimate of the most relevant motional parameters, which depend on the degree of structural order of the crystal packing. Moreover, the analysis of similar PBI pigments showed that the π-flip motion of the phenyl ring is strongly affected by the length of the alkyl linker with the PBI core.

By exploiting the detailed knowledge achieved in this work, we are planning to extend the combination of SSNMR experiments and DFT calculations to PBI pigments structurally slightly different from P-black (for instance, PR-190 and P-black L0096), also for those compounds which cannot be analyzed through single-crystal XRD. The collected molecular information could be combined with structural data of the same pigments on a larger length scale (obtained, for instance, by means of XRD and electronic microscopies) and with their NIR reflective and transparency performance. Such a system-

atic analysis could shed light on the factors mainly determining the success of a PBI "cool" pigment.

■ ASSOCIATED CONTENT

⑤ Supporting Information

The Supporting Information is available free of charge at https://pubs.acs.org/doi/10.1021/acs.jpcc.0c04940.

> Isotropic CSs, linewidths, and areas of the peaks obtained from the fitting of the experimental ^{13}C-selective spectra of P-black; theoretical values of ^{13}C and ^1H isotropic CS obtained from DFT calculations on P-black as an isolated molecule and in the crystal; $^1H-^{13}C$ HMQC spectrum of P-black; and variable temperature ^{13}C CP/MAS spectra of P-black-S (PDF)

■ AUTHOR INFORMATION

Corresponding Authors

Francesca Martini − *Dipartimento di Chimica e Chimica Industriale, Università di Pisa, 56124 Pisa, Italy; INSTM, UdR Pisa, 56124 Pisa, Italy; Centro per l'Integrazione della Strumentazione Scientifica dell'Università di Pisa (CISUP), 56126 Pisa, Italy; Istituto di Chimica dei Composti Organo Metallici, Consiglio Nazionale delle Ricerche (CNR-ICCOM), 56124 Pisa, Italy;* Phone: +390502219353; Email: francesca.martini@unipi.it

Marco Geppi − *Dipartimento di Chimica e Chimica Industriale, Università di Pisa, 56124 Pisa, Italy; INSTM, UdR Pisa, 56124 Pisa, Italy; Centro per l'Integrazione della Strumentazione Scientifica dell'Università di Pisa (CISUP), 56126 Pisa, Italy; Istituto di Chimica dei Composti Organo Metallici, Consiglio Nazionale delle Ricerche (CNR-ICCOM), 56124 Pisa, Italy;* ⓞ orcid.org/0000-0002-2422-8400; Phone: +390502219289; Email: marco.geppi@unipi.it

Authors

Giovanni Barcaro − *Istituto per i Processi Chimico-Fisici, Consiglio Nazionale delle Ricerche (CNR-IPCF), 56124 Pisa, Italy*

Susanna Monti − *Istituto di Chimica dei Composti Organo Metallici, Consiglio Nazionale delle Ricerche (CNR-ICCOM), 56124 Pisa, Italy;* ⓞ orcid.org/0000-0002-3419-7118

Luca Contiero − *Cromology Italia S.P.A., 55016 Porcari, Lucca, Italy*

Giacomo Ruggeri − *Dipartimento di Chimica e Chimica Industriale, Università di Pisa, 56124 Pisa, Italy; INSTM, UdR Pisa, 56124 Pisa, Italy*

Marco Lessi − *Dipartimento di Chimica e Chimica Industriale, Università di Pisa, 56124 Pisa, Italy; Centro per l'Integrazione della Strumentazione Scientifica dell'Università di Pisa (CISUP), 56126 Pisa, Italy*

Andrea Pucci − *Dipartimento di Chimica e Chimica Industriale, Università di Pisa, 56124 Pisa, Italy; INSTM, UdR Pisa, 56124 Pisa, Italy; Centro per l'Integrazione della Strumentazione Scientifica dell'Università di Pisa (CISUP), 56126 Pisa, Italy;* ⓞ orcid.org/0000-0003-1278-5004

Fabio Bellina − *Dipartimento di Chimica e Chimica Industriale, Università di Pisa, 56124 Pisa, Italy; INSTM, UdR Pisa, 56124 Pisa, Italy; Centro per l'Integrazione della Strumentazione Scientifica dell'Università di Pisa (CISUP), 56126 Pisa, Italy;* ⓞ orcid.org/0000-0002-4939-7008

Silvia Borsacchi − *Istituto di Chimica dei Composti Organo Metallici, Consiglio Nazionale delle Ricerche (CNR-ICCOM),*

56124 Pisa, Italy; Centro per l'Integrazione della Strumentazione Scientifica dell'Università di Pisa (CISUP), 56126 Pisa, Italy; orcid.org/0000-0003-3696-0719

Author Contributions

The manuscript was written through contributions of all authors. All authors have given approval to the final version of the manuscript.

Notes

The authors declare no competing financial interest.

■ REFERENCES

(1) Tian, Z.; Guo, Y.; Li, J.; Li, C.; Li, W. Benzodithiophene-Fused Perylene Bisimides as Electron Acceptors for Non-Fullerene Organic Solar Cells with High Open-Circuit Voltage. *ChemPhysChem* **2019**, *20*, 2696–2701.

(2) Matussek, M.; Filapek, M.; Gancarz, P.; Krompiec, S.; Grzegorz Małecki, J.; Kotowicz, S.; Siwy, M.; Maćkowski, S.; Chrobok, A.; Schab-Balcerzak, E.; et al. Synthesis and Photophysical Properties of New Perylene Bisimide Derivatives for Application as Emitting Materials in OLEDs. *Dyes Pigm.* **2018**, *159*, 590–599.

(3) Gupta, R. K.; Sudhakar, A. A. Perylene-Based Liquid Crystals as Materials for Organic Electronics Applications. *Langmuir* **2019**, *35*, 2455–2479.

(4) Wang, Z.; Wang, G.; Chang, X.; Liu, K.; Qi, Y.; Shang, C.; Huang, R.; Liu, T.; Fang, Y. A Perylene Bisimide-Contained Molecular Dyad with High-Efficient Charge Separation: Switchability, Tunability, and Applicability in Moisture Detection. *Adv. Funct. Mater.* **2019**, *29*, 1905295–1905310.

(5) Schiphorst, J. T.; Kendhale, A. M.; Debije, M. G.; Menelaou, C.; Herz, L. M.; Schenning, A. P. H. J. Dichroic Perylene Bisimide Triad Displaying Energy Transfer in Switchable Luminescent Solar Concentrators. *Chem. Mater.* **2014**, *26*, 3876–3878.

(6) Gutierrez, G. D.; Coropceanu, I.; Bawendi, M. G.; Swager, T. M. A Low Reabsorbing Luminescent Solar Concentrator Employing π-Conjugated Polymers. *Adv. Mater.* **2015**, *28*, 497–501.

(7) Carlotti, M.; Ruggeri, G.; Bellina, F.; Pucci, A. Enhancing Optical Efficiency of Thin-Film Luminescent Solar Concentrators by Combining Energy Transfer and Stacked Design. *J. Lumin.* **2016**, *171*, 215–220.

(8) Iasilli, G.; Francischello, R.; Lova, P.; Silvano, S.; Surace, A.; Pesce, G.; Alloisio, M.; Patrini, M.; Shimizu, M.; Comoretto, D.; et al. Luminescent Solar Concentrators: Boosted Optical Efficiency by Polymer Dielectric Mirrors. *Mater. Chem. Front.* **2019**, *3*, 429–436.

(9) Geervliet, T. A.; Gavrila, I.; Iasilli, G.; Picchioni, F.; Pucci, A. Luminescent Solar Concentrators Based on Renewable Polyester Matrices. *Chem.—Asian J.* **2018**, *14*, 877–883.

(10) Ciardelli, F.; Ruggeri, G.; Pucci, A. Dye-Containing Polymers: Methods for Preparation of Mechanochromic Materials. *Chem. Soc. Rev.* **2013**, *42*, 857–870.

(11) Carlotti, M.; Gullo, G.; Battisti, A.; Martini, F.; Borsacchi, S.; Geppi, M.; Ruggeri, G.; Pucci, A. Thermochromic Polyethylene Films Doped with Perylene Chromophores: Experimental Evidence and Methods for Characterization of Their Phase Behaviour. *Polym. Chem.* **2015**, *6*, 4003–4012.

(12) Donati, F.; Pucci, A.; Cappelli, C.; Mennucci, B.; Ruggeri, G. Modulation of the Optical Response of Polyethylene Films Containing Luminescent Perylene Chromophores. *J. Phys. Chem. B* **2008**, *112*, 3668–3679.

(13) Würthner, F. Perylene Bisimide Dyes as Versatile Building Blocks for Functional Supramolecular Architectures. *Chem. Commun.* **2004**, 1564–1579.

(14) Kaur, B.; Quazi, N.; Ivanov, I.; Bhattacharya, S. N. Near-Infrared Reflective Properties of Perylene Derivatives. *Dyes Pigm.* **2012**, *92*, 1108–1113.

(15) Qin, J.; Qu, J.; Song, J.; Song, Z.; Zhang, W.; Shi, Y.; Zhang, T.; Xue, X.; Zhang, R.; Zhang, H.; et al. The Optical Properties of Black Coatings and Their Estimated Cooling Effect and Cooling Energy Savings Potential. *J. Power Energy Eng.* **2014**, *02*, 68–75.

(16) Mazhar, M.; Abdouss, M.; Gharanjig, K.; Teimuri-Mofrad, R. Synthesis, Characterization and Near Infra-Red Properties of Perylenebisimide Derivatives. *Prog. Org. Coat.* **2016**, *101*, 297–304.

(17) Akbari, H.; Pomerantz, M.; Taha, H. Cool Surfaces and Shade Trees to Reduce Energy Use and Improve Air Quality in Urban Areas. *Sol. Energy* **2001**, *70*, 295–310.

(18) Cozza, E. S.; Alloisio, M.; Comite, A.; Di Tanna, G.; Vicini, S. NIR-Reflecting Properties of New Paints for Energy-Efficient Buildings. *Sol. Energy* **2015**, *116*, 108–116.

(19) Jose, S.; Joshy, D.; Narendranath, S. B.; Periyat, P. Recent Advances in Infrared Reflective Inorganic Pigments. *Sol. Energy Mater. Sol. Cells* **2019**, *194*, 7–27.

(20) Levinson, R.; Berdahl, P.; Akbari, H. Solar spectral optical properties of pigments-Part I: model for deriving scattering and absorption coefficients from transmittance and reflectance measurements. *Sol. Energy Mater. Sol. Cells* **2005**, *89*, 319–349.

(21) Synnefa, A.; Santamouris, M.; Apostolakis, K. On the Development, Optical Properties and Thermal Performance of Cool Colored Coatings for the Urban Environment. *Sol. Energy* **2007**, *81*, 488–497.

(22) Chakraborty, T.; Lee, X. A Simplified Urban-Extent Algorithm to Characterize Surface Urban Heat Islands on a Global Scale and Examine Vegetation Control on Their Spatiotemporal Variability. *Int. J. Appl. Earth Obs. Geoinf.* **2019**, *74*, 269–280.

(23) Sarrat, C.; Lemonsu, A.; Masson, V.; Guedalia, D. Impact of Urban Heat Island on Regional Atmospheric Pollution. *Atmos. Environ.* **2006**, *40*, 1743–1758.

(24) Muscio, A. The Solar Reflectance Index as a Tool to Forecast the Heat Released to the Urban Environment: Potentiality and Assessment Issues. *Climate* **2018**, *6*, 12–21.

(25) Levinson, R.; Berdahl, P.; Akbari, H. Solar spectral optical properties of pigments-Part II: survey of common colorants. *Sol. Energy Mater. Sol. Cells* **2005**, *89*, 351–389.

(26) Minei, P.; Lessi, M.; Contiero, L.; Borsacchi, S.; Martini, F.; Ruggeri, G.; Geppi, M.; Bellina, F.; Pucci, A. Boosting the NIR Reflective Properties of Perylene Organic Coatings with Thermoplastic Hollow Microspheres: Optical and Structural Properties by a Multi-Technique Approach. *Sol. Energy* **2020**, *198*, 689–695.

(27) Kaur, B.; Bhattacharya, S. N.; Henry, D. J. Interpreting the Near-Infrared Reflectance of a Series of Perylene Pigments. *Dyes Pigm.* **2013**, *99*, 502–511.

(28) Meymand, F. M.; Mazhar, M.; Abdouss, M. Investigation of Substituent Effect on Cool Activity of Perylene Bisimide Pigments. *J. Coat. Technol. Res.* **2019**, *16*, 439–447.

(29) Klebe, G.; Graser, F.; Hädicke, E.; Berndt, J. Crystallochromy as a Solid-State Effect: Correlation of Molecular Conformation, Crystal Packing and Colour in Perylene-3,4:9,10-Bis(Dicarboximide) Pigments. *Acta Crystallogr., Sect. B: Struct. Sci.* **1989**, *45*, 69–77.

(30) Hädicke, E.; Graser, F. Structures of Eleven Perylene-3,4:9,10-Bis(Dicarboximide) Pigments. *Acta Crystallogr., Sect. C: Cryst. Struct. Commun.* **1986**, *42*, 189–195.

(31) Martini, F.; Minei, P.; Lessi, M.; Contiero, L.; Borsacchi, S.; Ruggeri, G.; Geppi, M.; Bellina, F.; Pucci, A. Structural Order and NIR Reflective Properties of Perylene Bisimide Pigments: Experimental Evidences From a Combined Multi-Technique Study. *Dyes Pigm.* **2020**, *179*, 108401.

(32) Muniz-Miranda, F.; Minei, P.; Contiero, L.; Labat, F.; Ciofini, I.; Adamo, C.; Bellina, F.; Pucci, A. Aggregation Effects on Pigment

Coatings: Pigment Red 179 as a Case Study. *ACS Omega* **2019**, *4*, 20315−20323.

(33) Gisslén, L.; Scholz, R. Crystallochromy of Perylene Pigments: Influence of an Enlarged Polyaromatic Core Region. *Phys. Rev. B* **2011**, *83*, 1064−1067.

(34) Geppi, M.; Borsacchi, S.; Mollica, G.; Veracini, C. A. Applications of Solid-State NMR to the Study of Organic/Inorganic Multicomponent Materials. *Appl. Spectrosc. Rev.* **2009**, *44*, 1−89.

(35) Bryce, D. L. NMR Crystallography: Structure and Properties of Materials From Solid-State Nuclear Magnetic Resonance Observables. *IUCrJ* **2017**, *4*, 350−359.

(36) Hodgkinson, P. NMR Crystallography of Molecular Organics. *Prog. Nucl. Magn. Reson. Spectrosc.* **2020**, *118−119*, 10−53.

(37) Partridge, B. E.; Leowanawat, P.; Aqad, E.; Imam, M. R.; Sun, H.-J.; Peterca, M.; Heiney, P. A.; Graf, R.; Spiess, H. W.; Zeng, X.; et al. Increasing 3D Supramolecular Order by Decreasing Molecular Order. A Comparative Study of Helical Assemblies of Dendronized Nonchlorinated and Tetrachlorinated Perylene Bisimides. *J. Am. Chem. Soc.* **2015**, *137*, 5210−5224.

(38) Percec, V.; Peterca, M.; Tadjiev, T.; Zeng, X.; Ungar, G.; Leowanawat, P.; Aqad, E.; Imam, M. R.; Rosen, B. M.; Akbey, U.; et al. Self-Assembly of Dendronized Perylene Bisimides Into Complex Helical Columns. *J. Am. Chem. Soc.* **2011**, *133*, 12197−12219.

(39) Percec, V.; Hudson, S. D.; Peterca, M.; Leowanawat, P.; Aqad, E.; Graf, R.; Spiess, H. W.; Zeng, X.; Ungar, G.; Heiney, P. A. Self-Repairing Complex Helical Columns Generated via Kinetically Controlled Self-Assembly of Dendronized Perylene Bisimides. *J. Am. Chem. Soc.* **2011**, *133*, 18479−18494.

(40) Percec, V.; Sun, H.-J.; Leowanawat, P.; Peterca, M.; Graf, R.; Spiess, H. W.; Zeng, X.; Ungar, G.; Heiney, P. A. Transformation From Kinetically Into Thermodynamically Controlled Self-Organization of Complex Helical Columns with 3D Periodicity Assembled From Dendronized Perylene Bisimides. *J. Am. Chem. Soc.* **2013**, *135*, 4129−4148.

(41) Hansen, M. R.; Graf, R.; Sekharan, S.; Sebastiani, D. Columnar Packing Motifs of Functionalized Perylene Derivatives: Local Molecular Order Despite Long-Range Disorder. *J. Am. Chem. Soc.* **2009**, *131*, 5251−5256.

(42) Fung, B. M.; Khitrin, A. K.; Ermolaev, K. An Improved Broadband Decoupling Sequence for Liquid Crystals and Solids. *J. Magn. Reson.* **2000**, *142*, 97−101.

(43) Opella, S. J.; Frey, M. H. Selection of Nonprotonated Carbon Resonances in Solid-State Nuclear Magnetic Resonance. *J. Am. Chem. Soc.* **1979**, *101*, 5854−5856.

(44) Lesage, A.; Sakellariou, D.; Steuernagel, S.; Emsley, L. Carbon−Proton Chemical Shift Correlation in Solid-State NMR by Through-Bond Multiple-Quantum Spectroscopy. *J. Am. Chem. Soc.* **1998**, *120*, 13194−13201.

(45) Neue, G.; Dybowski, C. Determining Temperature in a Magic-Angle Spinning Probe Using the Temperature Dependence of the Isotropic Chemical Shift of Lead Nitrate. *Solid State Nucl. Magn. Reson.* **1997**, *7*, 333−336.

(46) Giannozzi, P.; Baroni, S.; Bonini, N.; Calandra, M.; Car, R.; Cavazzoni, C.; Ceresoli, D.; Chiarotti, G. L.; Cococcioni, M.; Dabo, I.; et al. QUANTUM ESPRESSO: a Modular and Open-Source Software Project for Quantum Simulations of Materials. *J. Phys.: Condens. Matter* **2009**, *21*, 395502−395520.

(47) Perdew, J. P.; Burke, K.; Ernzerhof, M. Generalized Gradient Approximation Made Simple. *Phys. Rev. Lett.* **1996**, *77*, 3865−3868.

(48) Grimme, S. Semiempirical GGA-Type Density Functional Constructed with a Long-Range Dispersion Correction. *J. Comput. Chem.* **2006**, *27*, 1787−1799.

(49) Pickard, C. J.; Mauri, F. All-Electron Magnetic Response with Pseudopotentials: NMR Chemical Shifts. *Phys. Rev. B* **2001**, *63*, 245101.

(50) Sottile, M.; Tomei, G.; Borsacchi, S.; Martini, F.; Geppi, M.; Ruggeri, G.; Pucci, A. Epoxy Resin Doped with Coumarin 6: Example of Accessible Luminescent Collectors. *Eur. Polym. J.* **2017**, *89*, 23−33.

(51) Williams, G.; Watts, D. C. Non-Symmetrical Dielectric Relaxation Behaviour Arising From a Simple Empirical Decay Function. *Trans. Faraday Soc.* **1970**, *66*, 80−85.

(52) Kaplan, J. I.; Garroway, A. N. Homogeneous and Inhomogeneous Distributions of Correlation Times. Lineshapes for Chemical Exchange. *J. Magn. Reson.* **1982**, *49*, 464−475.

(53) Garroway, A. N.; Ritchey, W. M.; Moniz, W. B. Some Molecular Motions in Epoxy Polymers: a Carbon-13 Solid-State NMR Study. *Macromolecules* **1982**, *15*, 1051−1063.

(54) Everatt, B.; Harris, R. K.; Kenwright, A. M.; Packer, K. J.; Stark, B. P. Investigation of Molecular Motions in a Derivative of Bisphenol-a Diglycidyl Ether by Variable-Temperature High-Resolution Solid-State Carbon-13 NMR. *Magn. Reson. Chem.* **1987**, *25*, 80−83.

(55) McConnell, H. M. Reaction Rates by Nuclear Magnetic Resonance. *J. Chem. Phys.* **1958**, *28*, 430−431.

(56) Resing, H. A. Apparent Phase-Transition Effect in the NMR Spin-Spin Relaxation Time Caused by a Distribution of Correlation Times. *J. Chem. Phys.* **1965**, *43*, 669−678.

(57) Carignani, E.; Borsacchi, S.; Geppi, M. Dynamics by Solid-State NMR: Detailed Study of Ibuprofen Na Salt and Comparison with Ibuprofen. *J. Phys. Chem. A* **2011**, *115*, 8783−8790.

(58) Weininger, U.; Modig, K.; Akke, M. Ring Flips Revisited: 13C Relaxation Dispersion Measurements of Aromatic Side Chain Dynamics and Activation Barriers in Basic Pancreatic Trypsin Inhibitor. *Biochemistry* **2014**, *53*, 4519−4525.

(59) Dreydoppel, M.; Raum, H. N.; Weininger, U. Slow ring flips in aromatic cluster of GB1 studied by aromatic 13C relaxation dispersion methods. *J. Biomol. NMR* **2020**, *74*, 183−191.

(60) Nall, B. T.; Zuniga, E. H. Rates and Energetics of Tyrosine Ring Flips in Yeast Iso-2-Cytochrome C. *Biochemistry* **1990**, *29*, 7576−7584.

(61) Twyman, J. M.; Dobson, C. M. Aromatic ring dynamics in crystalline penicillins from variable temperature 13C cross-polarisation magic-angle-spinning n.m.r. *J. Chem. Soc., Chem. Commun.* **1988**, *12*, 786.